THE ASTROPHYSICAL JOURNAL, 494:430–437, 1998 February 10

PROTON ACCELERATION NEAR AN X-TYPE MAGNETIC RECONNECTION REGION

KEN-ICHI MORI, JUN-ICHI SAKAI, AND JIE ZHAO
Laboratory for Plasma Astrophysics, Department of Electronics and Information, Faculty of Engineering, Toyama University, 3190, Gofuku, Toyama, 930 Japan
Received 1997 January 15; accepted 1997 August 29

ABSTRACT

We investigate the behavior of protons near an X-type magnetic reconnection region by numerical simulations. The magnetic field is taken to be hyperbolic and time stationary with a uniform electric field perpendicular to the magnetic field. We also study the effects of the magnetic field along the uniform electric field. We found from many parametric runs that the energy spectrum of accelerated protons near an X-type magnetic reconnection region is universal with a power-law spectrum $E^{-\gamma}$, where the power-law index γ is about 2.0–2.2. The acceleration time of protons with the energy range of 1–20 MeV is very rapid and within $\sim 10^2 \omega_{ci}^{-1}$, which is much less than 1 s for solar flare plasmas. We compare our results with some observations of solar flares.

Subject headings: MHD — Sun: flares — Sun: magnetic fields — Sun: X-rays, gamma rays

1. INTRODUCTION

Sakai & de Jager (1996) gave a review of the recent high-resolution observations of solar plasma loops with simulations of current-carrying loops and tried to arrive at the present understanding of solar flare phenomena. In chapter 7 of their review, they summarized the present understanding of high-energy particle acceleration processes during and after solar flares. There are two types of solar flares: confined/impulsive and eruptive/dynamic flares. Confined/impulsive flares are spatially compact, and as a fairly general rule they show impulsive hard X-ray and/or microwave bursts. Eruptive/dynamic flares, on the other hand, are spatially more extended and last longer. As proposed by de Jager (1988) and Sakai & de Jager (1991), there are three phases of acceleration in a fully developed eruptive/dynamic flare. The relevant observations regarding the first two phases are (1) the acceleration times of electrons and protons to energies of order 1 MeV are on the order of a second and (2) MeV protons are accelerated nearly simultaneously with MeV electrons. Many theoretical works (Forman, Ramaty, & Zweibel 1986; Simnett 1995) to explain the above observational requirements (for the review, see Sakai & de Jager 1996) have been done.

In the first phase of acceleration, current loop coalescence is one of the most plausible models of solar flares. Although the triggering mechanisms of most complex flares are still puzzling so far, several examples of solar flares triggered by current loop coalescence were observed by *Yohkoh* (for the review, see Sakai & de Jager 1996). In the case of partial reconnection of kink-unstable loop coalescence (Nishikawa et al. 1994), it seems that electrons can be promptly accelerated to relativistic energies, while the problem of proton acceleration has not been investigated because of the limitations of full proton dynamics by using a particle simulation model.

Sakai (1990) showed that, during three-dimensional X-type current loop coalescence and under suitable assumptions of the size and other physical parameters in the region of acceleration, protons and electrons may be accelerated promptly (i.e., within less than 1 s) to ≈ 100 GeV and ≈ 100 MeV, respectively. De Jager & Sakai (1991) showed that the duration of impulsive phase bursts (5–25 s) observed during the impulsive phases of flares can be explained quantitatively by the mechanism of X-type current-loop coalescence. Sakai (1992) developed a model for long-duration gamma-ray/proton flares ("gradual GR/P flares") in order to explain prompt proton and electron acceleration during the impulsive phase. He determined the electric fields during the implosion phase of the current sheet from the MHD equations and investigated the motion of test protons and electrons. Results showed that, under reasonable assumptions of the size and velocities in the reconnection area, both protons and electrons can be accelerated promptly within 1 s to ~ 70 MeV and ~ 200 MeV, respectively. However, the above previous works did not give the energy spectrum of accelerated particles.

Bulanov (1980) first showed the energy spectrum of accelerated particles in the simple X-type configuration near the reconnection region, which is given by $f(E) \sim \exp[-(E/E_0)^{3/4}]$ for $E \ll mc^2$. Deeg, Borovsky, & Duric (1991) investigated the same problem by using numerical simulation. Their results were in good agreement with the theory by Bulanov (1980). Nocera et al. (1996) investigated chaotic behavior of a particle motion in the same field configuration.

In the present paper we study the behavior of protons near an X-type magnetic reconnection region, which appears during current loop coalescence. We focus only on the local region of X-type reconnection region, where the magnetic field is hyperbolic and the electric field is produced by the plasma inflow during coalescence of two loops.

As pointed out by Sakai & Koide (1992), there are two types of magnetic reconnection during current loop coalescence: partial and complete magnetic reconnection. Fushiki & Sakai (1995) investigated both types of magnetic reconnection during coalescence of two current loops by using MHD simulation. Therefore, we investigate the effect of the magnetic field along the electric field induced by magnetic reconnection. We found from many parametric runs that the energy spectrum of accelerated protons near an X-type magnetic reconnection region is universal with a power-law spectrum $E^{-\gamma}$, where the power-law index γ is about 2.0–2.2. The acceleration time of protons with the energy range of 1–20 MeV is very rapid and within about $10^2 \omega_{ci}^{-1}$, which is much less than 1 s for solar plasmas.

The paper is organized as follows. In § 2 we present our

simulation model. In § 3 we show the simulation results. We summarize our results and compare them with some observations of solar flares in § 4.

2. SIMULATION MODEL

Magnetic reconnection during the coalescence of two current loops produces strong electric fields in the plasma and, as a result, charged particles can be accelerated. In this paper, we concentrate on the proton dynamics around an X-point. In this geometry, a homogeneous electric field couples with an inhomogeneous magnetic field. We consider an X-point with the following electric and magnetic configuration:

$$\boldsymbol{E} = (0, 0, E_z) , \quad \boldsymbol{B} = (\alpha y, \beta x, B_z) , \tag{1}$$

where E_z and B_z are the uniform z-components of the electric and magnetic fields, respectively, and α and β are the magnetic field gradients perpendicular to the z-axis.

The uniform electric field in the magnetic diffusion region could be generated by the Alfvénic motions of the inflow plasma and magnetic field in the external region. During the coalescence of two current loops, there are two types of magnetic reconnection that possibly occur: one is complete reconnection, where the B_z component is null; the other is partial magnetic reconnection, where the B_z-component is not null.

The normalized relativistic equations of the motion of a proton is given by

$$\frac{d\boldsymbol{u}}{dt} = \boldsymbol{E} + \frac{\boldsymbol{u} \times \boldsymbol{B}}{\Gamma} , \tag{2}$$

$$\frac{d\boldsymbol{x}}{dt} = \frac{R\boldsymbol{v}}{\Gamma} , \tag{3}$$

where the proton velocity $\boldsymbol{v} = \Gamma^{-1}\boldsymbol{u}$, the electric field $\boldsymbol{E}$, and the magnetic field $\boldsymbol{B}$ are normalized by Alfvén velocity V_A, $E_0 = V_A B_0/c$, and B_0, respectively. The time is normalized by the proton cyclotron frequency ω_{ci}, and the length is normalized by the distance over which the fields are aligned favorably for reconnection (L), respectively. The Lorentz factor Γ is given by $\Gamma = (1 + A^2\boldsymbol{u}^2)^{1/2}$, where $A = V_A/c$. The parameter R in equation (3) is defined by $R = V_A/(\omega_{ci} L)$.

To advance a particle under the guidance of electric and magnetic fields through solving the motion equation numerically, we desire a centered-difference form of the Newton-Lorentz equations of motion (Buneman 1993; Birdsall & Langdon 1991), namely,

$$\boldsymbol{u}^{\text{new}} - \boldsymbol{u}^{\text{old}} = \frac{q\,\delta t}{m}\left[\boldsymbol{E} + \frac{1}{2\Gamma}(\boldsymbol{u}^{\text{new}} + \boldsymbol{u}^{\text{old}}) \times \boldsymbol{B}\right], \tag{4}$$

where q is the charge of a particle, m is the mass of a particle, and δt is the calculate time step, respectively. As it stands, the equation for $\boldsymbol{u}^{\text{new}}$ is implicit. We choose the method proposed by Boris (1970) to obtain a simpler explicit solution using several steps that follow:

1. Half electric acceleration: $\boldsymbol{u}_0 = \boldsymbol{u}^{\text{old}} + q\boldsymbol{E}\,\delta t/2m$.
2. Pure magnetic rotation:

$$\boldsymbol{u}_1 = \boldsymbol{u}_0 + 2\,\frac{\boldsymbol{u}_0 + \boldsymbol{u}_0 \times \boldsymbol{b}_0}{1 + b_0^2} \times \boldsymbol{b}_0 ,$$

where $\boldsymbol{b}_0 = q\boldsymbol{B}\delta t/2m\Gamma$.

3. Another half electric acceleration: $\boldsymbol{u}^{\text{new}} = \boldsymbol{u}_1 + q\boldsymbol{E}\,\delta t/2m$.

This method produces rotation through an angle θ, where

$$\theta = 2 \arctan\left(\frac{qB}{m}\,\frac{\delta t}{2}\right). \tag{5}$$

The difference of θ to $\omega_c\,\delta t = qB\,\delta t/m$ is less than 1% error for $\omega_c\delta t < 0.35$. We can obtain highly accurate resolution even without taking very small time steps.

The system length in the x-, y-, z-directions is L. The domain is divided into $40 \times 40 \times 40$ grids, where the cell size (Δ) is $(1/40)L$. To avoid particles escaping in the x-y plane immediately after the external electric and magnetic fields are imposed, particles are located away from boundaries. Five mesh points are set to keep the margin in each side of the boundaries; i.e., particles are loaded in the region of $5 \le x \le 35$, $5 \le y \le 35$, $5 \le z \le 35$. In all, 30,000 protons are uniformly distributed in this region, hence the number density of particles is one per cell. The initial velocity distribution function for protons is Maxwellian with the thermal velocity $v_{\text{th}} = 0.1V_A$.

The simulation time step is $\omega_{ci}\,\delta t = 0.05$. The boundary conditions for protons are periodic in the z-direction and open in the x- and y-directions.

3. SIMULATION RESULTS

3.1. *Simulation Parameters and Summary*

In the simulation there are several important parameters. One is the ratio between the Alfvén velocity and the light velocity, which is taken to be $V_A/c = 10^{-2}$, The other is the parameter R appearing in equation (3), which is taken to be $R = 10^{-2}$. This means that the characteristic length of the reconnection region is about $L \approx 10^3\rho_i$, where ρ_i is the proton Larmor radius. In the following simulations we will fix the above two parameters. Other parameters that characterize the configuration of the reconnection region are the electric field (E_z) driven by magnetic reconnection, the magnetic field gradients in the x-and y-directions (α and β), and the magnetic field (B_z) along the electric field. The electric field driven by magnetic reconnection becomes large and sometimes exceeds unity when the inflow velocity into the reconnection region driven by attracting forces during current loop coalescence exceeds the local Alfvén velocity, which may correspond to explosive coalescence (see Sakai & Ohsawa 1987). The presence of the magnetic field component B_z coincides with the partial magnetic reconnection during current loop coalescence, while the complete reconnection case corresponds to $B_z = 0$. Table 1 summarizes all simulation runs.

3.2. *Complete Reconnection Case with $\alpha = \beta$*

Following the order in Table 1, we will describe the results with $\alpha = \beta = 0.05$ and $B_z = 0$ by changing the electric field E_z from 0.1 to 1.0. Figure 1*a* shows the vector plot of the magnetic field in the x-y plane. The proton energy spectra at $\omega_{ci}t = 100$ with different electric fields from 0.1 to 1.0 are shown in Figure 1*b*. As seen in Figure 1*b*, when the electric field is weak, the proton energy spectrum does not show a power law, but as the electric field becomes strong, the spectrum shows a power law with an index of about 2.0. Above $E_z = 0.3$, the power-law index is almost the same in all cases except for the high-energy part.

TABLE 1

SUMMARY OF SIMULATION RUNS

Magnetic Field Gradients	E_z	B_z
$\alpha = 0.05$, $\beta = 0.05$.....	0.1	0, 0.02, 0.05, 0.1
	0.2	0, 0.02, 0.05, 0.1
	0.3	0, 0.02, 0.05, 0.1
	0.5	0, 0.02, 0.05, 0.1
	1	0, 0.02, 0.05, 0.1
$\alpha = 0.1$, $\beta = 0.05$	0.5	0, 0.02, 0.05, 0.1
$\alpha = 0.2$, $\beta = 0.05$	0.5	0, 0.02, 0.05, 0.1
$\alpha = 0.05$, $\beta = 0.2$	0.5	0, 0.02, 0.05, 0.1

Figure 2 shows the time development of the proton distribution in the x-y plane with $E_z = 1.0$ and $\omega_{ci}t =$ (*a*) 0, (*b*) 25, (*c*) 50, and (*d*) 100. Figure 3 shows the phase spaces ([*a*] V_y-y plane and [*b*] V_x-x plane) of protons at $\omega_{ci}t = 100$, which corresponds to Figure 2*d*. As seen from Figures 2 and 3, the particles originally near the magnetic null point are accelerated. They leave their initial positions and accumulate at ± 5 from the null point in the y-direction. This movement is attributed to the production of high-energy particles, as seen in Figure 3. In other words, the most accelerated protons are located initially near magnetic null point.

3.3. *Partial Reconnection Case: $B_z \neq 0$*

In this subsection we study the effect of the magnetic field along the electric field E_z, which corresponds to partial magnetic reconnection during loop coalescence. Figure 4 shows the summary of proton energy spectra by varying the magnetic field B_z from 0 to 0.1 with $E_z = 0.5$ and $\alpha = \beta = 0.05$. As seen in Figure 4, the proton energy spectra show a power law, where the power indices for different runs keep a unique value that is approximately equal to 2. As the magnetic field B_z becomes strong, the number of accelerated protons increases.

3.4. *Effect of Asymmetric Magnetic Gradient on Energy Spectrum*

In this subsection we investigate the effect of an asymmetric gradient of the magnetic field in the x-y plane on the proton energy spectrum. Fixing the magnetic gradient in the y-direction (α), we changed the magnetic gradient in the x-direction (β). Figure 5 shows the proton energy spectrum with $E_z = 0.5$ and $B_z = 0.05$. As seen in Figure 5, the proton acceleration is most effective for the symmetric magnetic gradient ($\alpha = \beta = 0.05$), and the power-law index is almost independent of the magnetic field gradient near the magnetic reconnection region. Figure 6 shows magnetic field vectors in the x-y plane for two cases: (*a*) $\alpha = 0.2$, $\beta = 0.05$ and (*b*) $\alpha = 0.05$, $\beta = 0.5$, with $E_z = 0.5$ and $B_z = 0$. As seen in Figure 6*c*, the proton energy spectrum does not depend much on the asymmetry of the magnetic field gradient.

3.5. *High-Energy Proton Acceleration*

As seen in the previous subsections, the proton acceleration preferably occurs for strong electric field, symmetric magnetic gradient ($\alpha = \beta$) and for partial magnetic reconnection region ($B_z \neq 0$). Figure 7 shows the proton energy spectrum for $B_z = 0$ (*dotted curve*) and $B_z = 0.1$ (*solid curve*) with $E_z = 1.0$ and $\alpha = \beta = 0.5$. The proton energy spectra obtained for all parametric runs in the present simulations are well described by a power law with an index of about 2.0–2.2. It is interesting to compare the simulation result with the theoretical energy spectrum given by Bulanov (1980). Figure 8 shows comparison between the theory (*solid curve*) and the simulation result (*dotted curve*) with $B_z = 0.1$, $\alpha = \beta = 0.05$ and $E_z = 1.0$. The theoretical curve is given by $\ln f(E) = -0.023E^{3/4}$. As seen in Figure 8, the simulation result is in good agreement with the theoretical prediction in the high-energy range. Instead of the exponential dependence in the theory, however, our simulation shows that the proton energy spectrum is well described by a power law with an index of about 2.0–2.2. The maximum energy of the protons is about 20 MeV, if we take the Alfvén velocity $V_A \approx 3 \times 10^8$ cm s^{-1} in the solar flare region. The acceleration time $10^2\omega_{ci}^{-1}$ is about 10^{-4} s for a magnetic field of about 100 G, which is extremely rapid.

3.6. *Dependence on the Periodic Boundary Conditions*

In the simulations, the periodic boundary condition is used in the z-direction where the external electric field is imposed. One wonders whether the same protons would be continually accelerated several times since the particles encountering a boundary would reenter the computational box again at the other boundary. To resolve the argument, we estimate the number of particles encountering the boundaries in the z-direction. It is found that less than 1% of particles in the domain reach the boundaries once, but none encounter the boundaries twice within the duration of

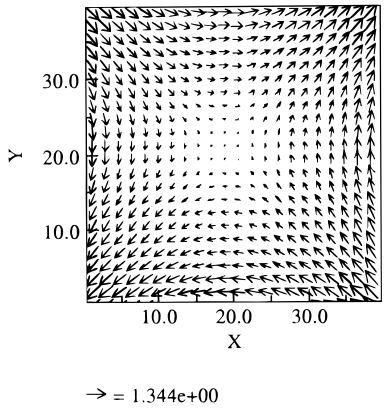

FIG. 1*a*

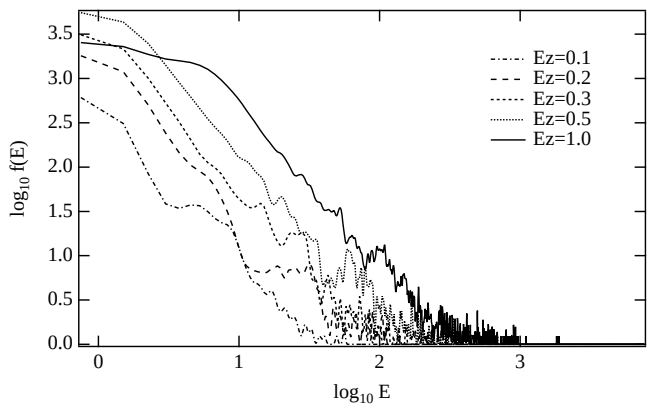

FIG. 1*b*

FIG. 1.—(*a*) Vector plot of the magnetic field in the x-y plane with $\alpha = \beta = 0.05$ and $B_z = 0$. (*b*) Proton energy spectra for various electric fields in the magnetic configuration (*a*), where the energy E is normalized by V_A^2.

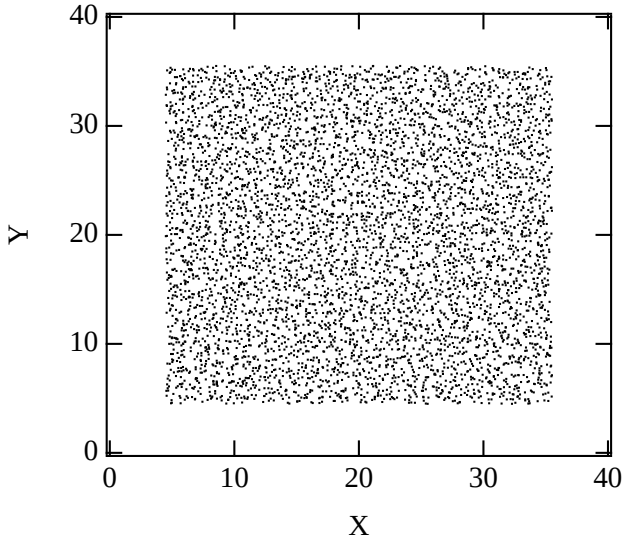

FIG. 2*a*

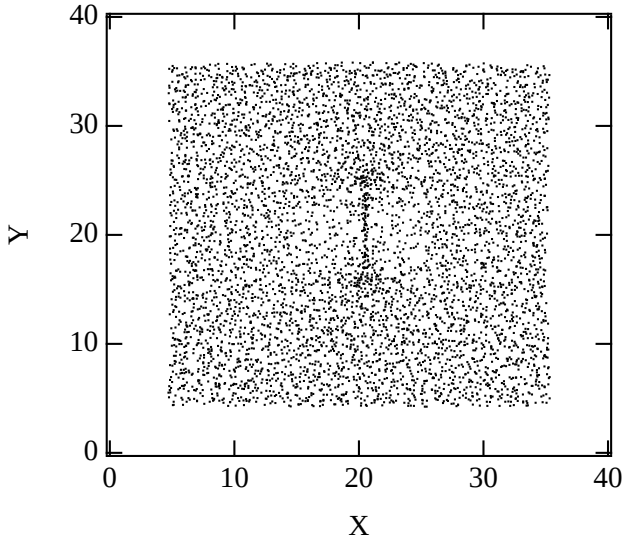

FIG. 2*b*

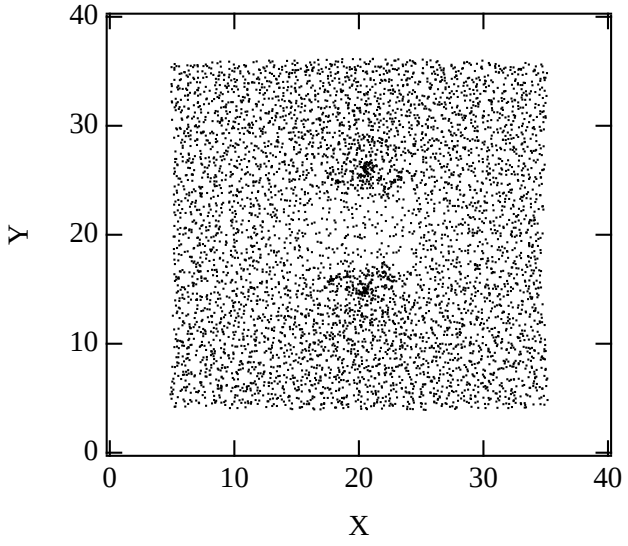

FIG. 2*c*

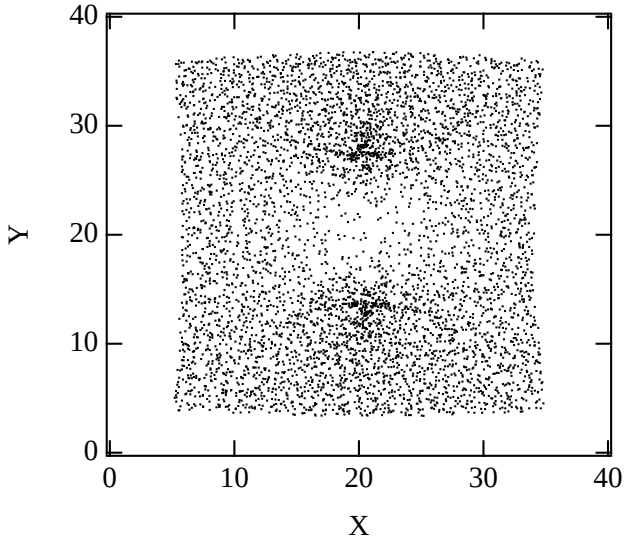

FIG. 2*d*

FIG. 2.—Time development of proton distributions in the x-y planes: $\omega_{ci}\, t$ = (*a*) 0, (*b*) 25, (*c*) 50, and (*d*) 100 with $E_z = 1.0$ and $B_z = 0$

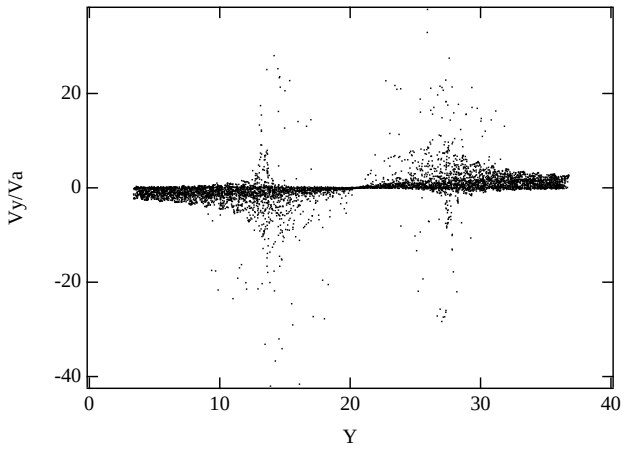

FIG. 3*a*

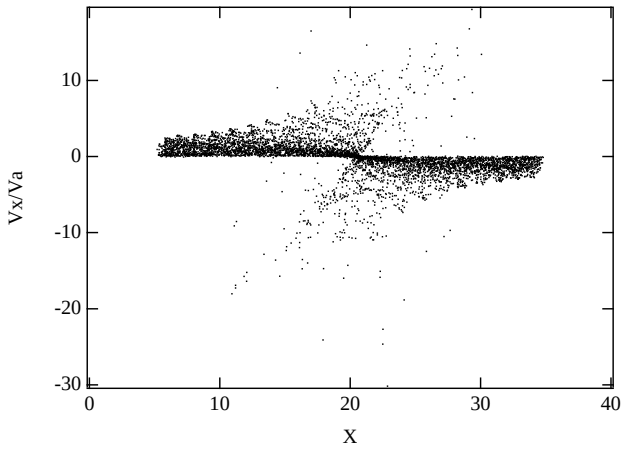

FIG. 3*b*

FIG. 3.—Snapshots of protons at $\omega_{ci}\, t = 100$ in the (*a*) V_y-y plane and in the (*b*) V_x-x plane, which corresponds to Fig. 2*d*

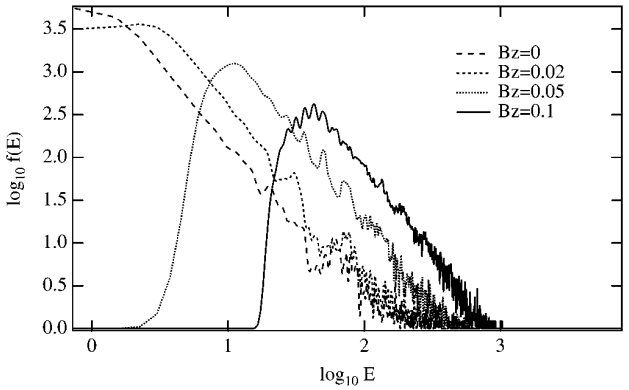

FIG. 4.—Proton energy spectra for various B_z with $E_z = 0.5$ and $\alpha = \beta = 0.05$ at $\omega_{ci} t = 100$. The energy E is normalized by V_A^2.

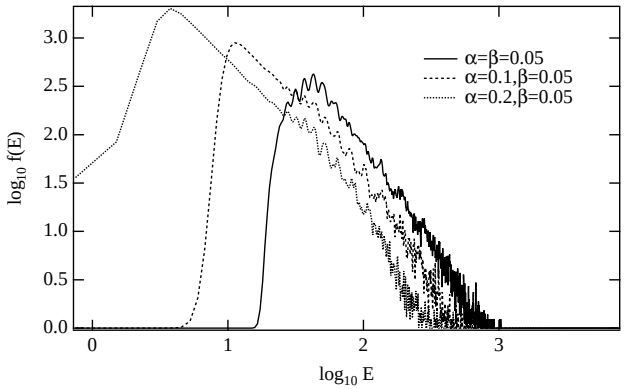

FIG. 5.—Proton energy spectra at $\omega_{ci} t = 100$ for various magnetic field gradients with $B_z = 0.05$ and $E_z = 0.5$. The energy E is normalized by V_A^2.

the simulations. The kinetic energy of this fraction of the particles is not in the high-energy range observed from the spectrum.

To rule out the influence of periodic boundary conditions on the proton spectrum, we performed an additional calculation in which the length in the z-direction is doubled, which corresponds to 80 grids, to prevent particles from reaching the boundaries. Initially particles are distributed within $15 \leq z \leq 45$, the same loading length as before.

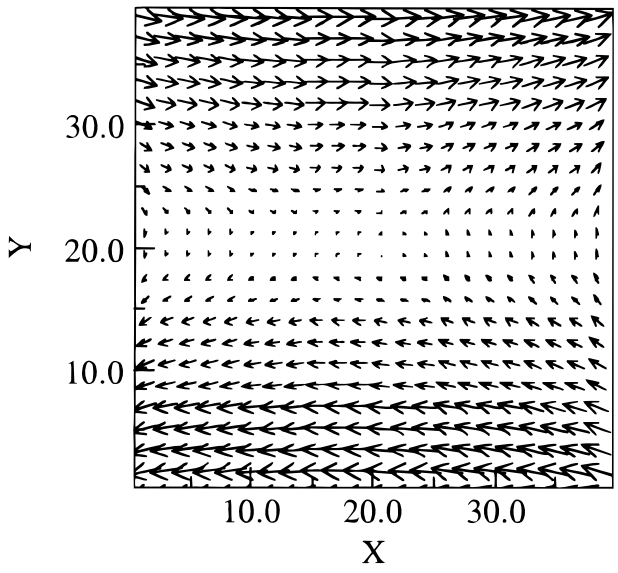

FIG. 6*a*

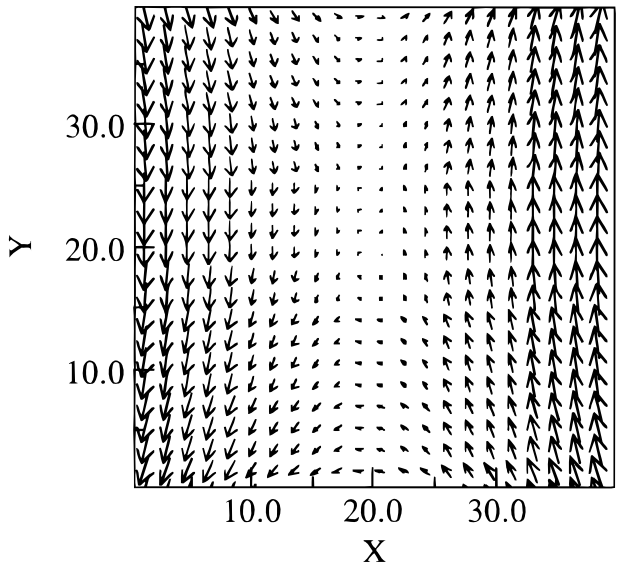

FIG. 6*b*

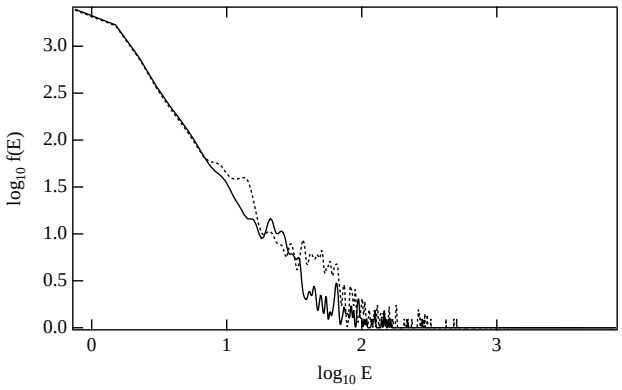

FIG. 6*c*

FIG. 6.—(*a*) Vector plot of the magnetic field in the x-y plane with $\alpha = 0.2$, $\beta = 0.05$, and $B_z = 0$. (*b*) Vector plot of the magnetic field in the x-y plane with $\alpha = 0.05$, $\beta = 0.2$, and $B_z = 0$. (*c*) Proton energy spectra at $\omega_{ci} t = 100$ for (*a*: *dotted curve*) and (*b*: *solid curve*). The energy E is normalized by V_A^2.

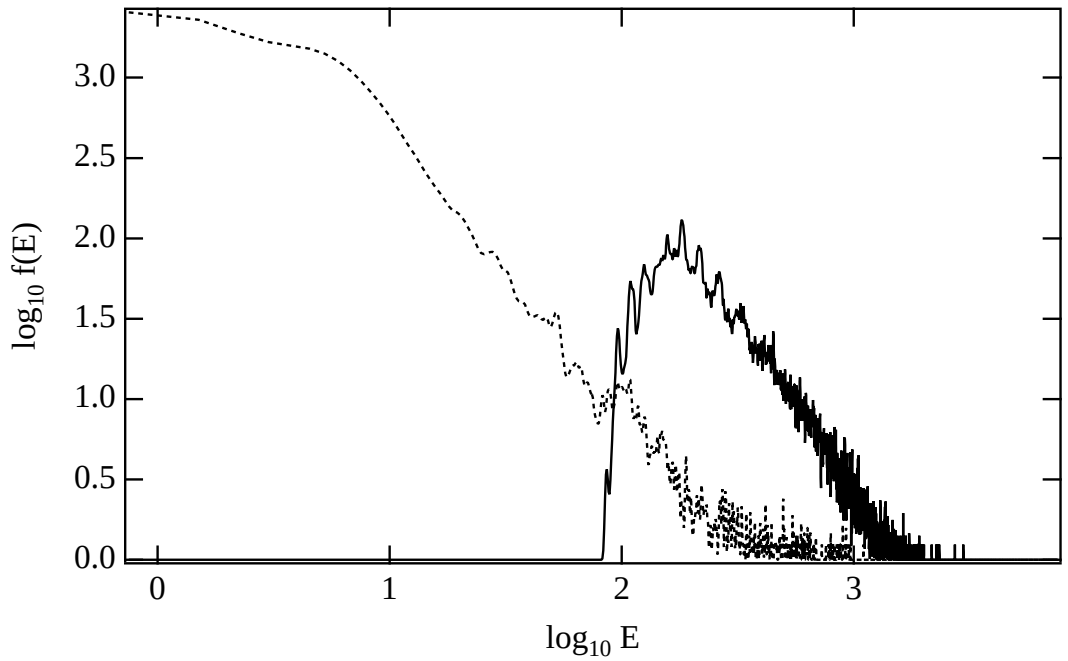

FIG. 7.—Proton energy spectra at $\omega_{ci}t = 100$ for $\alpha = \beta = 0.05, B_z = 0$ (*dotted curve*) and $B_z = 0.1$ (*solid curve*). The energy E is normalized by V_A^2.

Other parameters are the same as for Figure 8, which corresponds to the case with the strongest external electric field. Figure 9 (*top*) shows the snapshots of protons in the z-v_z phase, while Figure 9 (*bottom*) shows the proton spectrum at the end of simulation. It can be seen that none of the particles reach the boundaries. The spectrum is remarkably the same as that in Figure 8. This result implies that the fraction of the particles encountering the boundaries does not contribute much to the proton spectrum. Therefore, the use of periodic boundary conditions is unimportant to the spectrum.

3.7. *Dependence on the Magnitude of Alfvén Velocity*

As mentioned above, the two important parameters R and V_A, which are essential to the proton spectrum, are fixed for all simulation runs. The assumed Alfvén velocity of 3000 km s^{-1} is not surprisingly large or unreasonable for solar flares because it requires a magnetic field intensity of only 200 G even when the density is about $\sim 2 \times 10^{10}$ cm^{-3} (Masuda et al. 1994). For some solar physical conditions, however, the Alfvén velocity is widely taken to be 1000 km s^{-1}. It is instructive to investigate variations of the proton

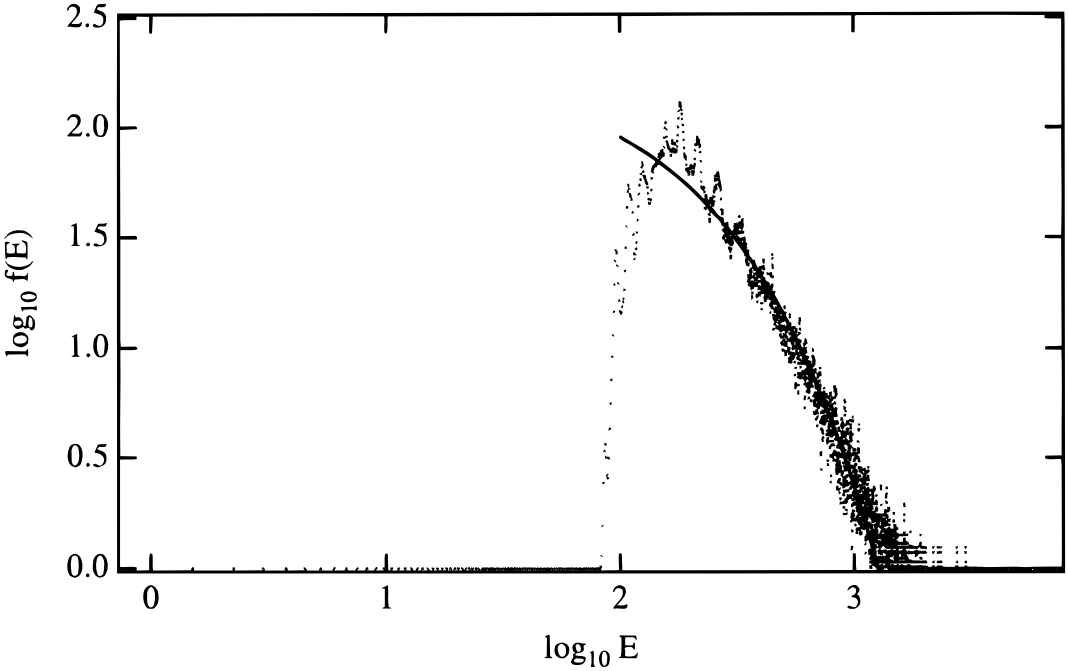

FIG. 8.—Comparison between theoretical curve $[\ln f(E) = -0.023E^{-3/4}]$ by Bulanov (1980) (*solid curve*) and simulation result (*dotted curve*) at $\omega_{ci}t = 100$ with $E_z = 1.0$, $B_z = 0.1$, and $\alpha = \beta = 0.05$. The energy E is normalized by V_A^2.

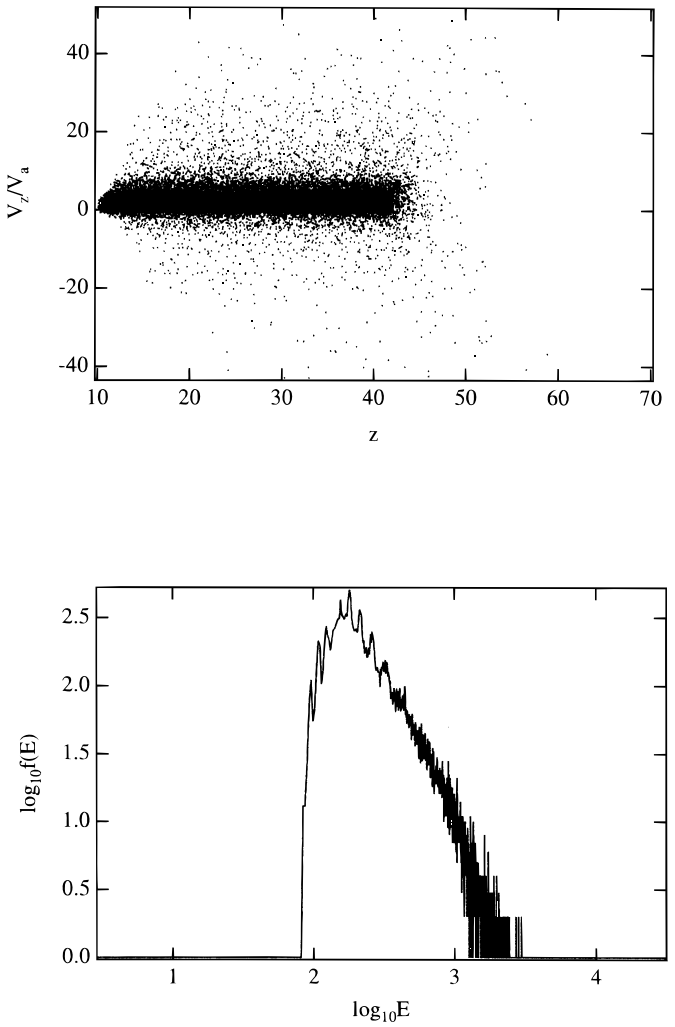

FIG. 9.—(*Top*) Snapshots of protons in the z-v_z plane and (*bottom*) its proton energy spectrum at $\omega_{ci}t = 100$ for the case with $E_z = 1.0$, $B_z = 0.1$, and $\alpha = \beta = 0.05$. The length in the z-direction is doubled, corresponding to 80 grids, while other parameters are kept the same.

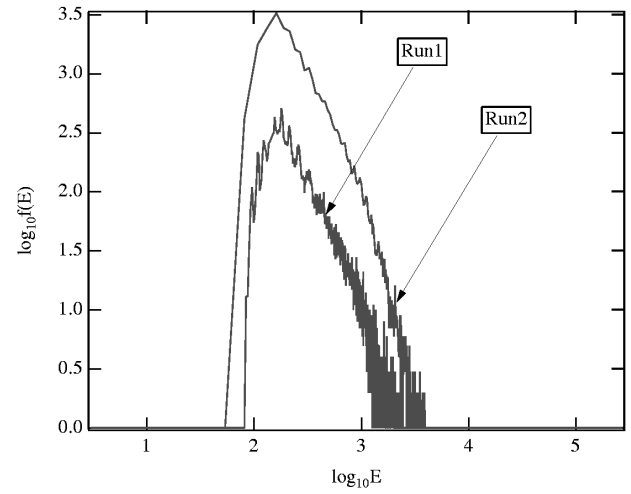

FIG. 10.—Proton energy spectra at $\omega_{ci}t = 100$ for different magnitudes of the Alfvén velocity. Run 1 is the case with $E_z = 1.0$, $B_z = 0.1$, and $\alpha = \beta = 0.05$, while run 2 is the case where the Alfvén velocity is one-third of that in run 1.

spectrum at different values of the Alfvén velocity. We compare the spectrum in Figure 8 with that when the Alfvén velocity is reduced to one-third, as shown in Figure 10.

It is clearly seen that the indices of the spectra vary little between the two cases. The proton spectrum therefore weakly depends on the value the Alfvén velocity. It indicates that our simulation results could be applicable to a wide range of solar physical conditions.

4. SUMMARY AND DISCUSSION

We have investigated the behavior of protons near an X-type magnetic reconnection region by numerical simulations. The magnetic field is taken to be hyperbolic and time stationary with an uniform electric field perpendicular to the magnetic field. We also studied the effects of a magnetic field component along the uniform electric field, which corresponds to partial magnetic reconnection during the coalescence of two current loops. We found from many parametric runs that the energy spectrum of accelerated protons near X-type magnetic reconnection regions is universal with a power-law spectrum $E^{-\gamma}$, where the power-law index γ is about 2.0–2.2. The acceleration time of protons is of the order of $10^2\omega_{ci}^{-1}$, which is much shorter than MHD timescale (about 1 s for solar physical conditions) during explosive magnetic reconnection.

Therefore the assumption that the magnetic and electric fields in the simulations are time stationary is justified.

Since the aim of this study is to investigate the acceleration of ions by magnetic reconnection in solar flares, we establish physical links between the scaling of the basic parameters in the simulations and solar flare conditions. As the initial given value of $R = V_A/c = 0.01$, the Alfvén velocity is 3000 km s^{-1}. Also, the ion thermal velocity is assumed to be equal to $0.1V_a$, or 300 km s^{-1}, which corresponds to the $\sim$900 eV ambient ions. The temperature is acceptable for a well-developed flare phase in a preflare phase. Assuming the coronal density of ions to be $\sim 10^{10}$ cm^{-3}, we derive an ion-cyclotron frequency of 1.34×10^6 rad s^{-1}, a magnetic field of 140 G, a system length of 0.23 km, and an acceleration time of 7.5×10^{-5} s, respectively. Those $\sim$900 eV ions can be accelerated to the MeV energy range, whose maximum is about $\sim$20 MeV. But the accelerated protons are not very numerous because only protons near the magnetic null can be accelerated. The above synthesis of the simulation parameters and results indicates that the acceleration of ions by magnetic reconnection is treated properly in the microscopic scale. The size of the reconnection region concerned is only 1000 times larger than the ion Larmor radius. We will study the same problem by performing simulations for larger scale configurations obtained from MHD simulation in future.

We compare our results with some observations of solar flares. Van Hollebeke, MaSung, & McDonald (1975) reported proton spectra, summarizing 185 solar proton events observed from *IMP-4* and *IMP-5* experimental data. They showed that these proton spectra approximately follow a power-law function in the 20–80 MeV range. The power-law index varies with time during a flare. The spectra also vary from flare to flare. Flares located away from the line magnetically connecting the Earth and the Sun exhibit steeper spectra. For flares located at heliolongitude W20–80, the power-law index determined at the time of maximum particle intensity is thought to be representative

of the source spectra. The power-law index is modified by the propagation effect at other times. For 32 flares located at W20–80, a power-law index in the 20–80 MeV range was shown by them. They gave seven events (7/32 = 22%) showing a spectral index of 1.8–2.2, which agrees with the present simulation result. Other events (78%) have an index in the range of 2.2–3.2, in which nine events show an index of 2.6–2.8.

Proton spectra in the energy range of 10–100 MeV can be derived from the ratio between 2.22 MeV (neutron capture line) to C and O de-excitation line fluences, which is the time-integrated flux. Ramaty et al. (1993) calculated the proton spectra using this method. Their conclusion is that most of the spectral indices are in the range of 3.0–4.6, which are harder than the present simulation result. Therefore, we still need further investigations to understand fully the proton acceleration mechanism(s) in the impulsive phase of solar flares, including turbulence effects due to current-driven instabilities and temperature anisotropy instabilities in the reconnection region.

We are thankful to Professor M. Yoshimori for his useful information about proton spectra. This work is partly supported by a Grant-in-Aid for Scientific Research from the Japan Ministry of Education (07640352). J. Zhao is grateful to Japan Society for the Promotion of Science for support.

REFERENCES

Birdsall, C. K., & Langdon, A. B. 1991, Plasma Physics via Computer Simulation (Bristol: Adam Hilger), 58
Boris, J. P. 1970, in Proc. Fourth Conf. Numer. Sim. Plasmas, November 2–3, Washington, DC, Naval Res. Lab., 3-67
Bulanov, S. V. 1980, Sov. Astron. Lett., 6, 206
Buneman, O. 1993, in Computer Space Plasma Physics, Simulation Techniques and Software, ed. H. Matsumoto & Y. Omura (Tokyo: Terra Scientific), 67
Deeg, H. J., Borovsky, J. E., & Duric, N. 1991, Phys. Fluids, B3, 2660
De Jager, C. 1988, Proc. 20th Cosmic Ray Conf. (Moscow), 7, 66
De Jager, C., & Sakai, J. I. 1991, Solar Phys., 133, 395
Forman, M. A., Ramaty, R., & Zweibel, E. G. 1986, in Physics of the Sun, vol. 2, ed. P. A. Sturrock, T. E. Holzer, D. M. Mihalas, & R. K. D. Ulrich (Dordrecht: Reidel), chap. 13
Fushiki, T., & Sakai, J. I. 1995, Solar Phys., 156, 265
Masuda, S., Kosugi, T., Hara, H., Tsuneta, T., & Ogawara, Y. 1994, Nature, 371, 497
Nishikawa, K. I., Sakai, J. I., Zhao, J., Neubert, T., & Buneman, O. 1994, ApJ, 434, 363
Nocera, L., Pegoraro, F., Bulanov, S. V., & Bertin, G. 1996, Physica Scripta, T63, 197
Ramaty, R., Mandzhavidze, N., Kozlovsky, B., & Skibo, J. G. 1993, Adv. Space Res., 13(9), 275
Sakai, J. I. 1990, ApJS, 73, 321
———. 1992, Solar Phys., 140, 99
Sakai, J. I., & de Jager, C. 1991, Solar Phys., 134, 329
———. 1996, Space Sci. Rev., 77, 1
Sakai, J. I., & Koide, S. 1992, Solar Phys., 142, 399
Sakai, J. I., & Ohsawa, Y. 1987, Space Sci. Rev., 46, 113
Simnett, G. M. 1995, Space Sci. Rev., 73, 387
Van Hollebecke, M. A. I., MaSung, L. S., & McDonald, F. B. 1975, Solar Phys., 41, 189